Struct Multidisc Optim (2010) 42:693–705
DOI 10.1007/s00158-010-0516-8

RESEARCH PAPER

A multifidelity approach for the construction of explicit decision boundaries: application to aeroelasticity

Christoph Dribusch · Samy Missoum · Philip Beran

Received: 28 October 2009 / Revised: 22 April 2010 / Accepted: 2 May 2010 / Published online: 12 June 2010

Abstract This paper presents a multifidelity approach for the construction of explicit decision boundaries (constraints or limit-state functions) using support vector machines. A lower fidelity model is used to select specific samples to construct the decision boundary corresponding to a higher fidelity model. This selection is based on two schemes. The first scheme selects samples within an envelope constructed from the lower fidelity model. The second technique is based on the detection of regions of inconsistencies between the lower and the higher fidelity decision boundaries. The approach is applied to analytical examples as well as an aeroelasticity problem for the construction of a nonlinear flutter boundary.

Keywords Support vector machines · Multifidelity · Flutter boundary

1 Introduction

The construction of explicit constraints or limit state functions (referred to as decision boundaries) using support vector machines (SVMs) has been used recently for design optimization or uncertainty quantification (Basudhar et al. 2008; Basudhar and Missoum 2008). One of the main attractions of SVMs lies in the possibility of representing the boundaries of disjoint and non-convex infeasible or failure domains. In addition, because the boundaries are explicit in terms of the design variables, optimization and probability of failure calculation are simplified.

The notion of *explicit design space decomposition (EDSD)* was introduced to circumvent the difficulties due to discontinuous behaviors (e.g., structural impact (Basudhar and Missoum 2009; Missoum et al. 2007)) and binary problems (Missoum et al. 2008; Layman et al. 2007). Also, because the construction of explicit boundaries is based on designs of experiments (DOE), an adaptive sampling scheme was introduced to reduce the number of required function evaluations and the total computational cost (Basudhar and Missoum 2008). Problems with traditional random variables as well as random fields were treated (Basudhar and Missoum 2009) with this approach.

For this reason, multifidelity approaches, whereby a hierarchy of model fidelities (from low to high) are used to describe the behavior of a system (Robinson et al. 2006; Eldred and Dunlavy 2006), appear as a natural complement to the adaptive sampling scheme. Fidelity qualifies the ability of a model to reproduce accurately, spatially and temporally, a phenomenon (e.g., aeroelastic behavior). A lower to medium fidelity model might be in the form of an analytical expression or a reduced order model (ROM) (Lucia et al. 2004). A high fidelity model could involve a full nonlinear structural finite element model with nonlinear aerodynamics. The lower fidelity models typically provide information on the "general behavior" of the system whose description is subsequently refined through the high fidelity model.

The advantages of using models of various fidelity have long been recognized in design optimization with a sig-

C. Dribusch · S. Missoum (✉)
Aerospace and Mechanical Engineering Department,
The University of Arizona, Tucson, AZ 85721, USA
e-mail: smissoum@email.arizona.edu

P. Beran
Air Force Research Laboratory, Wright-Patterson Air Force Base,
Building 146, 2210 Eighth Street, Dayton, OH 45433, USA

nificant number of publications on the topic. A review article (Simpson et al. 2008) provides some key studies in that area. It is noteworthy that a large part of the work on multifidelity is related to the use of surrogates such as response surfaces and metamodels (Simpson et al. 2008). Also, in most studies two levels of fidelity are used.

To point only to a few of the proposed approaches, techniques based on model "correction" are of particular importance. In this type of approaches, a surrogate is modified to match a high(er) fidelity model at specific points (e.g., the iterate during an optimization process). The matching is done so that the low and high fidelity models are equal at those points. This zero order "consistency" (Alexandrov et al. 2000a, b) has also been extended to first and second order consistencies (Eldred et al. 2004; Eldred and Dunlavy 2006). The modifications can be carried out based on additive or multiplicative corrections (Alexandrov et al. 2000a, b; Eldred et al. 2004; Eldred and Dunlavy 2006). It is also possible to build a surrogate correction function which is then applied to low fidelity response to approximate the high fidelity response. This was successfully demonstrated by several authors (Mason 1998; Balabanov et al. 1998; Venkataraman et al. 1998; Vitali et al. 1998; Madsen and Langthjem 2001; Keane 2003; Gano et al. 2005, 2006). The method was generalized by Toropov and Markine (Toropov and Markine 1996). They suggested three ways of tuning a low fidelity model to the high fidelity model. The tuning parameters are obtained by minimizing the discrepancy between the high fidelity responses and the tuned low fidelity responses at sampling points.

Another important contribution to the multifidelity area, is the use of trust regions that enable one to quantify the quality of an approximation during an optimization. This was used by Alexandrov et al. (2000a, b) who developed an approximation and model management framework (AMMF). This was later extended by Eldred et al. (2004), Eldred and Dunlavy (2006) in conjunction with model corrections.

In this paper, a low fidelity model and a high fidelity model are used to build an accurate explicit decision boundary corresponding to the high fidelity model. The proposed methodology, described in detail in Section 3 is based on SVMs only, which gives the ability to treat discontinuous and binary problems, and, if desired, mix computational and experimental data. As an example of practical application of the methodology, the proposed methodology can be used, as done in this article, for the construction of aeroelastic flutter boundaries. These boundaries split the space into stable and unstable configurations, thus fitting perfectly the EDSD framework.

The multifidelity approach uses two techniques to draw information from a lower fidelity model to help the construction of a higher fidelity SVM-based decision function:

– The low fidelity decision boundary can be used to define a region, referred to as the "envelope", outside of which the model can be evaluated with the lower fidelity model only. The goal is to reduce the number of function evaluations compared to a design of experiments performed over the whole space.
– The two decision boundaries are inconsistent in certain regions which are, because of the SVM-based construction of the boundaries, efficiently identifiable. Locating samples in these regions might carry valuable information to update the high fidelity boundary.

In this article, for the sake of completeness, the "envelope" approach and the detection of inconsistent regions are also mixed with another update scheme solely based on the higher fidelity model such as the one presented in earlier studies (Basudhar and Missoum 2008).

The methodology is demonstrated on analytical functions (with a higher and a lower fidelity "model"). The approach is also applied to the construction of a nonlinear and linear flutter boundary for a two degree of freedom airfoil. For this problem, the high fidelity model has nonlinear stiffness properties and the lower fidelity model is linear.

This paper is constructed as follows. Section 2 provides a background on EDSD. The information presented in Section 2 gives the basic elements necessary to the understanding of the overall multifidelity methodology, described in detail in Section 3. Section 4 provides the results for the analytical and aeroelasticity problems.

2 Explicit design space decomposition (EDSD)

The objective of EDSD (Basudhar et al. 2008; Harrison et al. 2006) is to obtain an analytical "indicator" function $s(\mathbf{x})$, such that $sign(s(\mathbf{x}))$ indicates if a sample $\mathbf{x}$ is in the infeasible (failure) region(s). In order to construct the boundary $s(\mathbf{x}) = 0$, SVMs (Cristianini and Schölkopf 2002; Alpaydin 2004) were found to be the most suitable classifier. SVMs are widely used in the computer science community. They can reproduce nonlinear, disjoint region boundaries in multidimensional spaces. An SVM is constructed from a "machine learning" process, based only on classified samples. An SVM provides an analytical expression for the boundary which is efficiently evaluated and makes it suitable for uncertainty quantification and optimization. Another strong advantage of EDSD with SVMs is the possibility to manage various failure modes simultaneously.

Specifically, consider a set of N training points $\mathbf{x}_i$. Each point is associated with one of two classes characterized by a value $y_i = \pm 1$. A general expression of the SVM is:

$$s(\mathbf{x}) = b + \sum_{i=1}^{N} \lambda_i y_i K(\mathbf{x}_i, \mathbf{x}) \tag{1}$$

where the Lagrange multipliers λ_i and the scalar b are determined by quadratic programming optimization. Several types of Kernel, K, exist such as polynomial, gaussian, radial basis etc. (Cristianini and Schölkopf 2002). For instance, a polynomial Kernel of degree p is:

$$K(\mathbf{x}_i, \mathbf{x}) = (1 + \langle \mathbf{x}_i, \mathbf{x} \rangle)^p \tag{2}$$

Note that only a fraction of the Lagrange multipliers λ_i are nonzero. The corresponding training points are called support vectors. The accuracy of the SVM in predicting the correct class depends on the number and distribution of the training points. The number of training points is limited by the cost of evaluating a model response. For the selection of samples, two approaches are described in the following two subsections.

2.1 Predefined (static) sampling

In this basic approach, a DOE is used to train the SVM. The choice of DOE is essential as the samples should be distributed as uniformly as possible. This aspect is essential to avoid lack or redundancy of information in certain regions of the design space. The approach referred to as Centroidal Voronoi Tesselation (CVT) is of particular interest (Romero et al. 2006).

2.2 Adaptive sampling

Due to the so-called "curse of dimensionality", the use of a static design of experiments might lead to large errors in high dimensions. For this reason, an adaptive sampling scheme was proposed (Basudhar et al. 2008). Of particular importance, the accuracy of the SVM boundary is improved by locating samples on or close to the actual boundary and away from existing samples. This approach represents one step of the proposed algorithm in Basudhar et al. (2008), but this very step will also be used in the multifidelity approach presented in this paper. That is, the main idea is to place each additional sample on the current approximation of the boundary, at maximum distance to other training points. The distance to the closest training point is given by (3). The new training point $\mathbf{x}^*$ is now given by (4). Together these two equations describe a max/min optimization problem. The basic adaptive sampling algorithm is given in Algorithm 1.

$$d_{min}(\mathbf{x}, \mathbf{x}_i) = \min_i \|\mathbf{x}_i - \mathbf{x}\| \tag{3}$$

$$\mathbf{x}^* = \arg\max_{\mathbf{x}} d_{min}(\mathbf{x}, \mathbf{x}_i) \qquad s.t. \quad s(\mathbf{x}) = 0 \tag{4}$$

Algorithm 1 Adaptive Sampling

```
procedure ADAPTIVESAMPLING
    select initial training points
    train SVM
    repeat
        add training point(s) near boundaries
        train SVM
    until Convergence
end procedure
```

3 Multifidelity approach

This work investigates the construction of an SVM decision boundary corresponding to a high fidelity model. In an initial step a low fidelity model is used to construct a low fidelity SVM s_{lf} using predefined sampling (Section 2.1). The low fidelity SVM is not modified and the low fidelity model is not used again after this initial step. The high fidelity (HF) SVM corresponds to the high fidelity model, but not all training points for the HF SVM are classified through the HF model. The high fidelity SVM is initially close to the low fidelity SVM, but refined iteratively as detailed in this section. The low fidelity boundary defined by $s_{lf}(\mathbf{x}) = 0$ is used in the selection and classification of training points for the high fidelity SVM in two main ways:

- An envelope around the low fidelity boundary is defined. The motivation behind the envelope is the assumption that the low fidelity SVM will correctly classify any sample that is far from the actual high fidelity boundary. That is, any training samples created within this envelope will be classified using the high fidelity model while samples on and outside of the boundaries of the envelope are classified through the low fidelity SVM (Fig. 1). The definition of the envelope around the low fidelity boundary is quite involved and is described in detail in Section 3.1.
- The low fidelity boundary is compared to the current approximation of the high fidelity boundary. Points of high discrepancy are selected as additional training

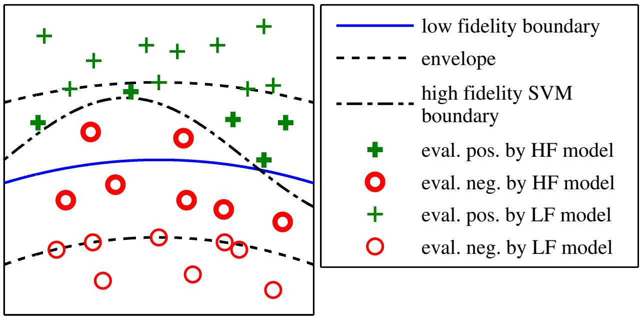

Fig. 1 Envelope approach: an envelope is defined around the low fidelity (LF) boundary. Each sample is evaluated as either positive (pos.) or negative (neg.). Samples inside the envelope are evaluated through the high fidelity (HF) model. Samples on and outside of the envelope are classified based on the low fidelity model

samples to train the high fidelity SVM. These training points are classified through the high fidelity model (Fig. 2). Detecting points of high discrepancy between the low fidelity SVM and the current high fidelity SVM is detailed in Section 3.2.

In addition to the use of the low fidelity SVM, the algorithm, described in detail in the following sections, is complemented by the sample selection scheme based on the maximum minimum distance presented in Section 2.2 and given by (4). This combination is outlined in Section 3.3.

3.1 Envelope approach

One of the major challenges of the envelope approach is to determine the margin. The margin determines the width of the envelope as described later in (6). Obviously the envelope should be wide enough to enclose the actual high fidelity boundary, which of course is unknown. On the other hand, it should be as narrow as possible to take advantage of the low fidelity model. This calls for an adaptive scheme to decide on the margin of the envelope. This is outlined in Algorithm 2. Only at steps 4 and 6 are samples evaluated through the high fidelity model. The steps of this algorithm are described in detail in Section 3.1.1. Figure 3 is a flow chart of the complete adaptive sampling process using envelopes.

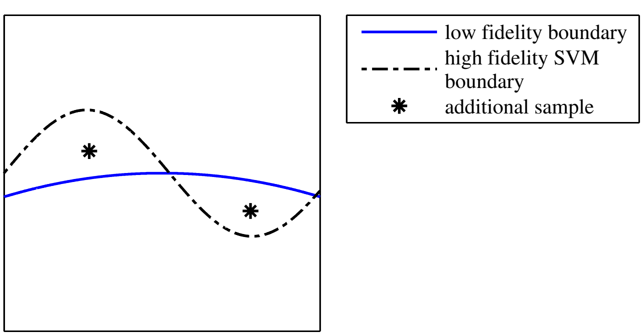

Fig. 2 Points of high discrepancy between the high fidelity SVM boundary and the low fidelity boundary are selected as additional training points for the high fidelity SVM

Algorithm 2 Envelope Approach

procedure ENVELOPEAPPROACH
  select initial margin ▹ Step 1
  define envelope ▹ Step 2
  add training points on boundary of envelope ▹ Step 2
  repeat
    train SVM ▹ Step 3
    add training point(s) inside envelope (HF eval.) ▹ Step 6
    if envelope is too narrow **then** ▹ Step 4
      discard training points on boundary of envelope ▹ Step 4
      discard envelope ▹ Step 4
      increase margin ▹ Step 4
      define envelope ▹ Step 2
      add training points on boundary of envelope ▹ Step 2
    end if
  until Convergence ▹ Step 5
end procedure
procedure DEFINEENVELOPE(margin)
  find base points x_b on current SVM boundary ▹ Step 2a
  generate envelope samples ▹ Step 2b
  create upper and lower SVM ▹ Step 2c
end procedure

It is noteworthy that in the proposed algorithm, the margin can only increase. This might seem *a priori* like a limitation. However, the envelope is always constructed from the fixed lower fidelity boundary. In addition, the margin is constant over the whole space. Therefore, if one starts with a small enough margin, there is be no need for its reduction.

3.1.1 Detailed steps of the envelope algorithm

1. *Selection of an Initial Margin for the Envelope*
   The margin m of the envelope represents our expectation of how close the actual high fidelity boundary will be to the low fidelity boundary. The hypothesis is that samples further than a certain distance (half the margin) away from the low fidelity boundary are correctly classified by the low fidelity SVM. (Note: If the initial margin is too small, it will be updated. On the other hand, if the initial margin is chosen too large, the reduction in the number of evaluated samples due to the use of

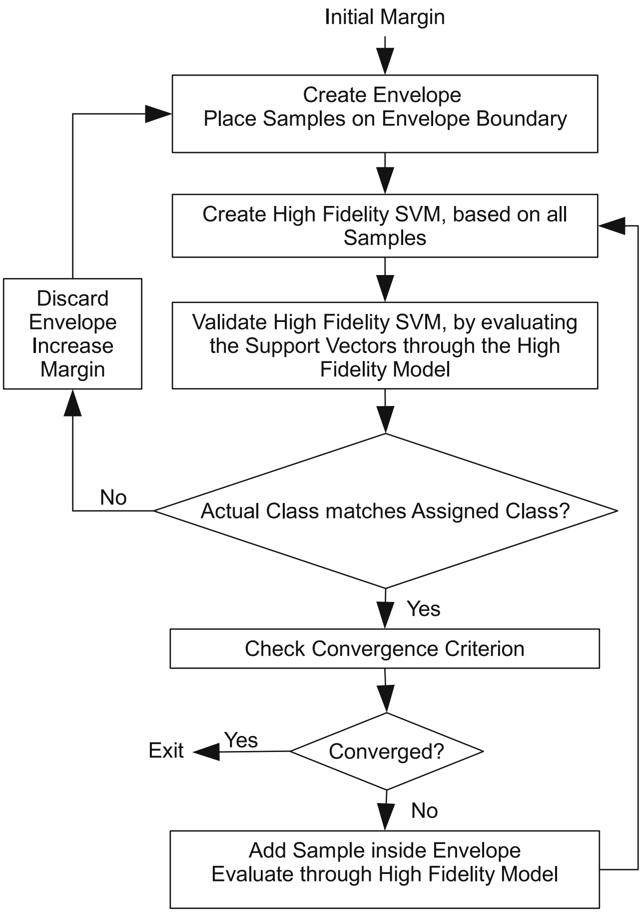

Fig. 3 Flow chart of the envelope process

low fidelity model will not be as significant as it could be.)

2. *Define the Envelope*
The envelope is defined by two SVMs, the lower SVM $s_l(\mathbf{x})$ and the upper SVM $s_u(\mathbf{x})$. $s_l(\mathbf{x}) = 0$ defines the boundary of the envelope in the feasible domain. $s_u(\mathbf{x}) = 0$ defines the boundary of the envelope in the infeasible domain. These SVMs are set up such that any sample inside the envelope is classified as negative by both SVMs. The lower and upper SVM are obtained in the following steps.

(a) *Find Base Points* ($\mathbf{x}_b$)
The base points $\mathbf{x}_{bi}$ are evenly distributed samples on the low fidelity boundary. They are determined sequentially. The first base point is added somewhere on the boundary, for example closest to the center of the design space. The location of each additional base point $\boldsymbol{x}_b^*$ is found by maximizing the distance to the closest existing base point while constraining the new base point $\boldsymbol{x}_b^*$ to lie on the SVM boundary. This is a global optimization problem (5).

$$
\begin{aligned}
\boldsymbol{x}_b^* = \arg\max_{\mathbf{x}} \; & d_{min}(\mathbf{x}, \mathbf{x}_{bi}) \\
s.t. \quad & s_{lf}(\mathbf{x}) = 0 \\
& \mathbf{x}_{min} \leq \mathbf{x} \leq \mathbf{x}_{max}
\end{aligned}
\tag{5}
$$

(b) *Generate Envelope Samples*
In order to create the envelope boundary, two envelope samples are generated from each base point. The two envelope samples are located on opposite sides of the low fidelity boundary. The distance between the two envelope samples equals the margin of the envelope. The first envelope sample ($\mathbf{x}_{e1}$) is located from the base point in the direction of the gradient of the low fidelity SVM at the base point. The second envelope sample ($\mathbf{x}_{e2}$) is located from the base point in the direction opposite to the gradient of the low fidelity SVM (6, Fig. 4). Values are assigned to the envelope samples, by evaluating them through the low fidelity SVM. This results in positive envelope samples on the infeasible side of the low fidelity SVM and negative envelope samples on the feasible side.

$$
\begin{aligned}
\mathbf{x}_{e1} &= \mathbf{x}_b + \frac{m}{2}\frac{\nabla s_{lf}(\mathbf{x}_b)}{\|\nabla s_{lf}(\mathbf{x}_b)\|} \\
\mathbf{x}_{e2} &= \mathbf{x}_b - \frac{m}{2}\frac{\nabla s_{lf}(\mathbf{x}_b)}{\|\nabla s_{lf}(\mathbf{x}_b)\|}
\end{aligned}
\tag{6}
$$

(c) *Create Upper and Lower SVMs*
The upper and lower SVMs represent the boundaries of the envelope. For every positive envelope sample, two training samples ($\mathbf{x}_u^+$ and $\mathbf{x}_u^-$) for the upper SVM are generated. The envelope sample itself cannot be used as a training sample, since it is located exactly on the boundary. Along the gradient of the low fidelity SVM, the two samples are located on either side and at a small distance ε to each other. $\mathbf{x}_u^-$ is the sample closer to the low

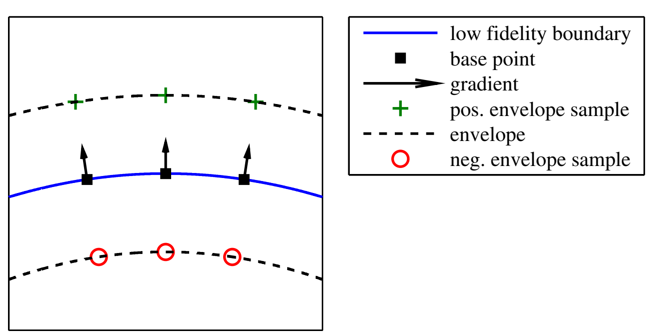

Fig. 4 Base points on the low fidelity SVM and envelope samples

fidelity boundary. The same procedure is repeated for the lower SVM, using the negative envelope samples (7). For the purpose of training the lower and the upper SVMs, the samples are assigned values corresponding to their superscript. This ensures that points inside the envelope are classified as negative by both the upper and the lower SVM. Figure 5 shows both the lower and the upper SVM and their training sets.

$$\begin{aligned}
\mathbf{x}_u^+ &= \mathbf{x}_{e1} + \varepsilon \frac{\nabla s_{lf}(\mathbf{x}_b)}{\|\nabla s_{lf}(\mathbf{x}_b)\|} \\
\mathbf{x}_u^- &= \mathbf{x}_{e1} - \varepsilon \frac{\nabla s_{lf}(\mathbf{x}_b)}{\|\nabla s_{lf}(\mathbf{x}_b)\|} \\
\mathbf{x}_l^+ &= \mathbf{x}_{e2} - \varepsilon \frac{\nabla s_{lf}(\mathbf{x}_b)}{\|\nabla s_{lf}(\mathbf{x}_b)\|} \\
\mathbf{x}_l^- &= \mathbf{x}_{e2} + \varepsilon \frac{\nabla s_{lf}(\mathbf{x}_b)}{\|\nabla s_{lf}(\mathbf{x}_b)\|}
\end{aligned} \tag{7}$$

3. *Create High Fidelity SVM*
An SVM approximation of the high fidelity boundary is constructed. It is based both on the envelope samples with their assigned values and on any other training points that have been evaluated through the high fidelity model (during previous iterations of the following steps 4 and 6). Figure 6 shows the high fidelity SVM. We are using here the hypothesis that the values assigned to the envelope samples are correct. In other words this new SVM is a prediction of the high fidelity SVM. The validity of the prediction will be checked in the next step.
4. *Validate High Fidelity SVM*
Only the training points which are support vectors affect the shape of the high fidelity SVM boundary. To validate the high fidelity SVM, we evaluate the support vectors through the high fidelity model. If the results match the values assigned in step 2b, then our hypothesis was good and we continue to the next step. Otherwise the hypothesis is wrong and the values assigned to the envelope samples are not reliable. Therefore the envelope samples are discarded and a new envelope is defined with a larger margin (return to step 2b).
5. *Check Convergence Criterion*
Check the convergence of the high fidelity SVM by monitoring the relative change with respect to the previous high fidelity SVM. Continue to step 6 as necessary. If the high fidelity SVM has converged sufficiently, switch to the next higher level of fidelity, if applicable. That means the current high fidelity SVM becomes the new low fidelity SVM and the whole process is repeated to build a new higher fidelity SVM. Figure 9 gives an example of a high fidelity SVM, that has almost converged.
6. *Add Training Point inside Envelope*
An additional training point $\mathbf{x}^*$ is found by maximizing the distance to the closest existing training point while constraining $\mathbf{x}^*$ to remain in the envelope. That is, the sample is classified as negative by both the lower and the upper SVM. The corresponding optimization problem is given by (8).

$$\begin{aligned}
\mathbf{x}^* &= \arg\max_{\mathbf{x}} d_{min}(\mathbf{x}, \mathbf{x}_i) \\
s.t. \quad & s_u(\mathbf{x}) \le 0 \\
& s_l(\mathbf{x}) \le 0 \\
& \mathbf{x}_{min} \le \mathbf{x} \le \mathbf{x}_{max}
\end{aligned} \tag{8}$$

The additional sample is evaluated through the high fidelity model. Return to step 3. Figure 7 shows the SVM after adding another sample (after step 3). One of the envelope samples has now become a support vector and must be evaluated in step 4.

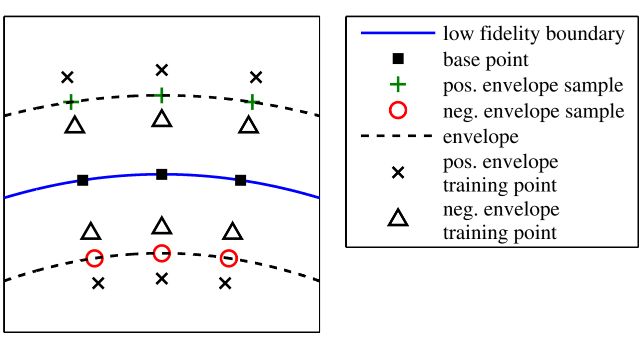

Fig. 5 Upper envelope SVM and lower envelope SVM, defining the envelope. Representation of the training samples used to generate them

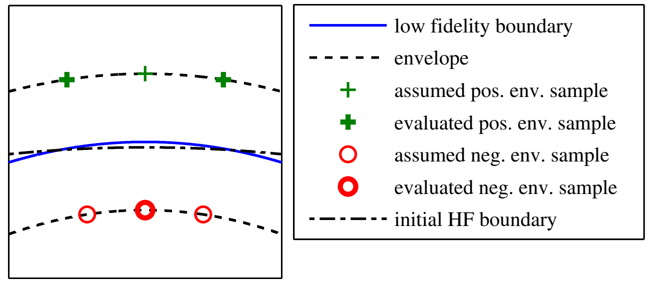

Fig. 6 High fidelity SVM, obtained from step 4. In this figure, no sample has yet been added inside the envelope. Therefore the high fidelity SVM is close to the low fidelity SVM

3.2 Detection of regions of high discrepancy

As a starting assumption, the "global" trends of the lower and higher fidelity models are similar: The lower fidelity model will actually enhance the definition of the explicit

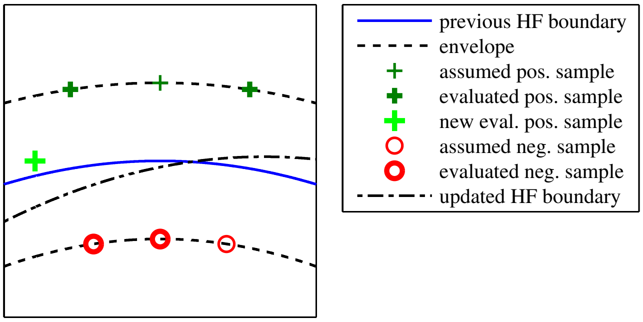

Fig. 7 High fidelity SVM, obtained from step 4 (during second iteration). One sample has been added in the envelope. A new SVM was created in step 3. Next (step 4) the envelope sample at the bottom left corner had to be evaluated through the high fidelity model, since it had become a support vector

boundary corresponding to the high fidelity model. This assumption leads to the natural conclusion: There exists a maximum inconsistency region between the two models. For SVMs, this corresponds to regions of highest likelihood of misclassification between the low and high-fidelity SVMs. The point of maximum likelihood of misclassification can be found with the following optimization problem:

$$\begin{aligned} &\min_{\mathbf{x}} \quad s_{lf}(\mathbf{x}) s_{hf}(\mathbf{x}) \\ &s.t. \quad \mathbf{x}_{min} \leq \mathbf{x} \leq \mathbf{x}_{max} \end{aligned} \tag{9}$$

Because the product of SVM functions might have many local optima, this is a global optimization problem. Problem (9), whose solution $\mathbf{x}^*$ is in general unique, enables the detection of "highly-dimensional pockets" characterized by a lack of data. Once the location of this sample is determined, the output of the higher fidelity model is obtained to enhance the quality of the previous classification. Note that if additional samples located in the pocket do not reduce the pocket size then this means that a systematic departure between the low and high fidelity boundaries has been reached, which is expected. In that case the classification of $\mathbf{x}^*$ will not modify s_{hf} significantly and a new solution $\mathbf{x}^*_{k+1}$ at iteration $k+1$ will be very close to $\mathbf{x}^*_k$. To avoid unnecessary function evaluations a measure of distance to existing samples is included in the optimization problem (10).

$$\begin{aligned} \mathbf{x}^* = \arg\min_{\mathbf{x}} \quad & s_{lf}(\mathbf{x}) s_{hf}(\mathbf{x}) \\ s.t. \quad & \left\| \mathbf{x} - \mathbf{x}_j \right\| \geq d_{crit} \quad j = 1 \ldots N \\ & \mathbf{x}_{min} \leq \mathbf{x} \leq \mathbf{x}_{max} \end{aligned} \tag{10}$$

d_{crit} is an arbitrary minimum distance. In this study, d_{crit} is a fraction of the envelope margin m:

$$d_{crit} = \frac{1}{4} m \tag{11}$$

Due to the critical distance constraint (10) the optimization problem eventually becomes infeasible. In that case the corresponding sample is ignored.

3.3 Combined selection of training points

In order to update the high fidelity SVM, it might be possible to reach better accuracy in less iterations by combining the various approaches to generate samples. Specifically, one can choose a combination of the envelope approach (8), the maxmin algorithm (4) and the detection of discrepancy approach (10). When all the approaches are used, (8) is used to obtain the first additional training point. Equation (4) is used to obtain the second training point. Equation (10) is used to obtain the third training point and so forth.

3.4 Convergence measure

In the general case, the error measure might not be available as the actual true boundary is not known. That is a convergence measure cannot be built based on the error. However, one can check the convergence by quantifying the relative changes in the SVM from one iteration to the next. For this purpose, a large number M of comparison points $\mathbf{x}_{ci}$ is generated over the whole space using Latin Hypercube Sampling (LHS). The convergence measure is the fraction of comparison points that is classified differently by the two SVMs. Equation (12) gives the convergence measure ε for two SVMs s_1 and s_2 and uses the fact that, if a sample is classified differently by the two SVMs, the product of the two SVM values is negative.

$$\varepsilon(s_1, s_2) = \frac{1}{M} \sum_{i=1}^{M} \frac{1}{2} \left(1 - \operatorname{sign}\left(s_1(\mathbf{x}_{ci}) s_2(\mathbf{x}_{ci})\right)\right) \tag{12}$$

3.5 Error measure

For analytical problems, the error between the approximated and the actual boundary can be calculated. The same measure as for convergence (12) can be used between the two boundaries.

4 Results

Two sets of results are presented on two distinct classes of problems:

– Analytical lower and higher fidelity models. In Section 4.1 both the high and the low fidelity model are analytical two-dimensional functions. Various combinations of sample selection techniques are compared in terms of the number of function calls to the high fidelity model.

– Nonlinear aeroelasticity problem with a two degree of freedom airfoil. In Section 4.2 the combination of the three approaches is used to obtain the nonlinear flutter boundary of a two degree of freedom airfoil with nonlinear stiffness terms. A lower fidelity model provides the linear flutter boundary.

For these examples, no convergence threshold was set. However, the convergence of the algorithm was studied by monitoring the error and the relative change in SVM for a reasonably large number of iterations. The SVMs were constructed using a polynomial kernel. Other choices of kernel have provided similar results. For the polynomial kernel, the lowest possible degree larger than one was chosen. This was done in order to obtain the "simplest" SVM that is able to classifiy its training data.

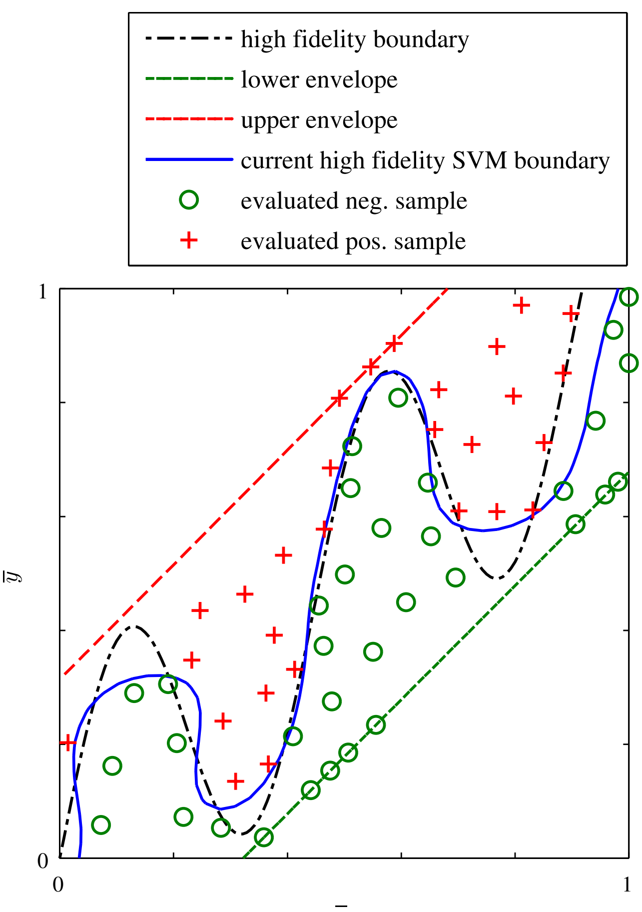

Fig. 8 High fidelity SVM (*blue*) and high fidelity model (*black*) after 75 samples (*dots*) have been evaluated. The upper and lower SVM are shown in *red* and *green*

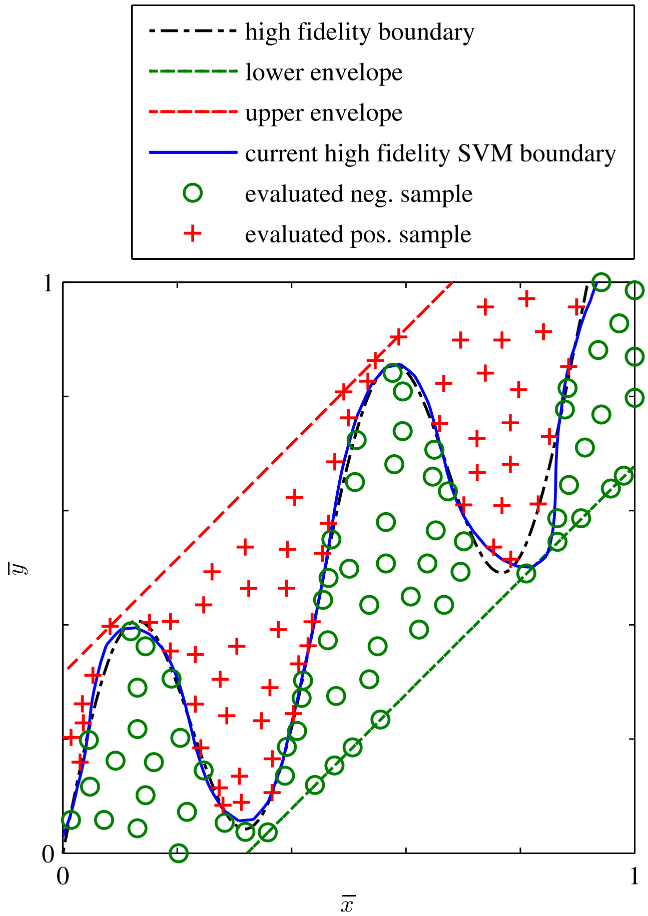

Fig. 9 High fidelity SVM (*blue*) and high fidelity model (*black*) after 150 samples (*dots*) have been evaluated. The upper and lower SVM are shown in *red* and *green*

4.1 Analytical functions

In this section the analytical function for the lower fidelity model is: $f_{lf}(x, y) = y - x$. The feasible domain is defined by $f_{lf}(x, y) < 0$. The function for the higher fidelity model is: $f_{hl}(x, y) = y - (x + 2\sin(2x))$. The feasible domain is defined by $f_{hl}(x, y) < 0$. The design space is given by $0 \leq x, y \leq 7$. The design space is normalized to $0 \leq \bar{x}, \bar{y} \leq 1$. The objective is to reconstruct the boundary corresponding to the higher fidelity model. These functions respect the requirement that there exists a distance d such that any sample, further than d away from the low fidelity boundary is classified identically by both the low and the high fidelity model. The boundary corresponding to the low fidelity model is of course the straight line $y(x) = x$, but to test the methodology, the low fidelity boundary was instead obtained from an SVM of the low fidelity model.

4.1.1 Envelope approach only

In this section, the analytical problem was considered with the envelope approach only (Section 3.1). It is understood

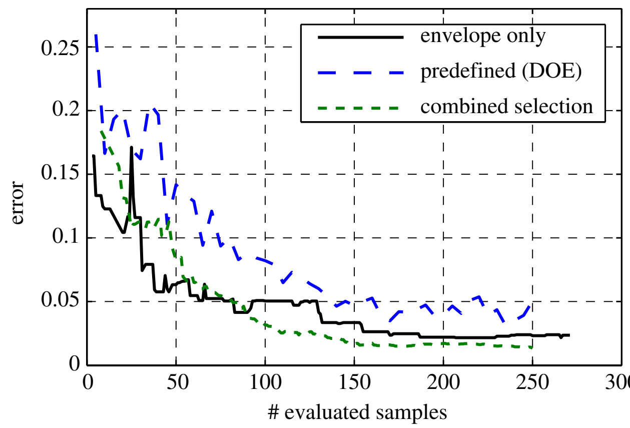

Fig. 10 Error of the high fidelity SVM, with respect to the number of evaluated samples. The combination of approaches (*green*) performs best. The envelope only (*black*) is consistently more efficient than a simple DOE on the whole space (*blue*)

Table 1 Airfoil parameters

Initial plunge ξ (0)	0.0
Initial plunge velocity ξ' (0)	0.0
Initial pitch α (0)	$-15° - 15°$
Initial pitch velocity α' (0)	$0° - 2.5°$
Reduced velocity U_R	$3.0 - 9.0$
Mass ratio μ	100.0
Natural frequency ratio ω	0.2
Elastic axis-mid chord separation a_h	-0.5
Center of mass - elastic axis separation x_α	0.25
Radius of gyration r_α	0.5
Pitch cubic stiffness β_α	-3.0
Plunge cubic stiffness β_ξ	0.0
Damping in pitch and plunge	0
Linear reduced flutter speed	6.29

that the envelope approach is best suited to provide a broad approximation of the higher fidelity SVM. However, the purpose of this example is to investigate the evolution of the error between the current approximation of the high fidelity SVM boundary and the actual high fidelity boundary as a function of the number of samples evaluated through the high fidelity model. The evolution of the error of the high fidelity SVM is shown by a solid black line in Fig. 10.

4.1.2 Combined selection approach

Here the combined selection approach (Section 3.3) is used. Figure 10 compares the achieved accuracy of the combination of approaches and of the envelope only approach. For reference, they are also compared to a regular DOE (Centroidal Voronoi Tesselation) on the whole design space (Section 2.1). The combination of approaches achieves the highest accuracy. The envelope only is consistently more efficient than a regular DOE on the whole space and even outperforms the combination on the first 50 samples. Figure 8 shows the approximated boundary after 75 evaluations through the high fidelity model. Figure 9 shows the approximated boundary after 150 evaluations through the high fidelity model.

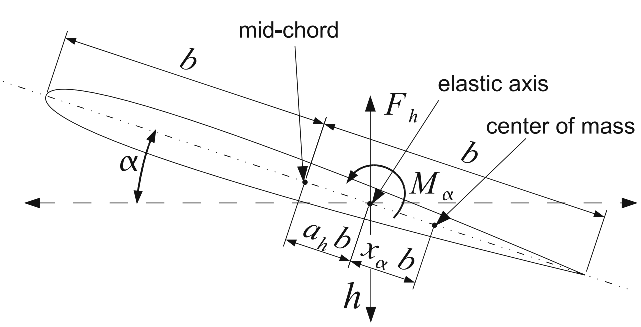

Fig. 11 Description of the two degree of freedom airfoil (Lee et al. 1999). The restoring forces due to the nonlinear springs are denoted by F and M. Their formulation is given in Appendix A

4.2 Two degree of freedom airfoil problem

4.2.1 Aeroelastic problem definition

The methodology is applied to a two degree of freedom (pitch and plunge) airfoil problem (Fig. 11). A rigid airfoil subject to incompressible flow is supported by translational

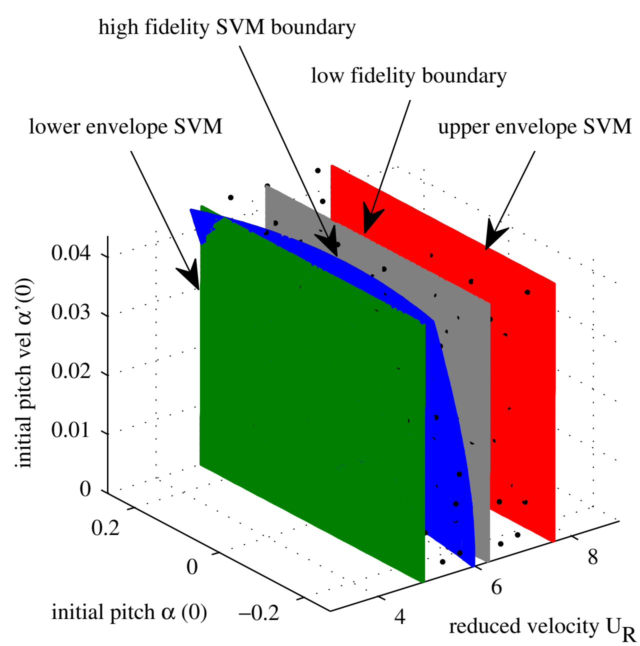

Fig. 12 Three-dimensional nonlinear flutter boundary, defines the values for reduced velocity, initial pitch angle and initial pitch velocity for which stable and flutter responses are encountered

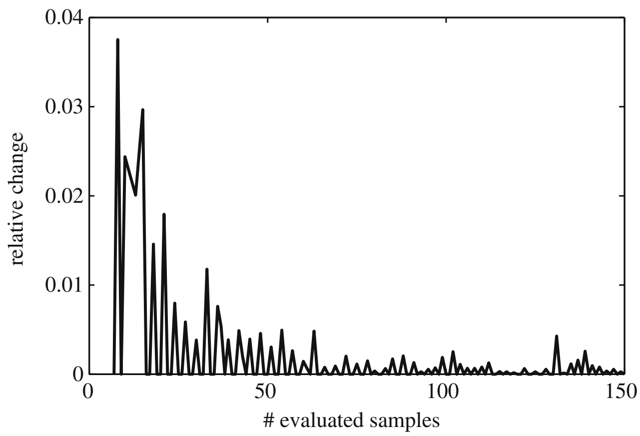

Fig. 13 Convergence of the three dimensional flutter boundary. This graph shows the relative change in the high fidelity SVM from one iteration to the next

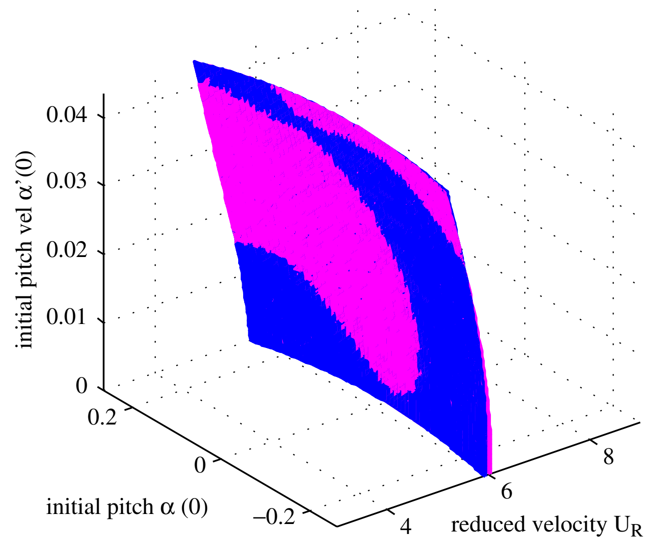

Fig. 15 Reference flutter boundary (*blue*) obtained from 5,000 grid samples and approximated boundary (*magenta*) obtained from the multifidelity approach after 150 samples

and rotational springs. This mechanism is described and analyzed in great detail by Lee et al. (1999).

The objective is to construct the flutter boundary as a function of initial pitch conditions and reduced velocity in the case of an airfoil with nonlinear stiffnesses. The "higher" fidelity model includes cubic stiffness terms, which makes the equations of motion nonlinear. The "lower" fidelity model has linear springs and its behaviour is described by a linear system of differential equations. For the lower fidelity model, the flutter velocity is independent of the initial conditions.

The flutter boundaries are constructed by investigating the stability of the airfoil using the time response (Appendix A). This classification is valid for the nonlinear and linear case. Note that in the linear case, the stability classification could also be achieved using a spectral analysis of the Jacobian (Lee et al. 1999; Seydel 1988). The simulation parameters used in the experiments are given in Table 1. The fixed parameters were chosen to match the values presented by Lee et al. (1999).

4.2.2 *Definition of nonlinear flutter boundary*

Figure 12 shows the three dimensional flutter boundary for the configuration given in Table 1. The configuration is

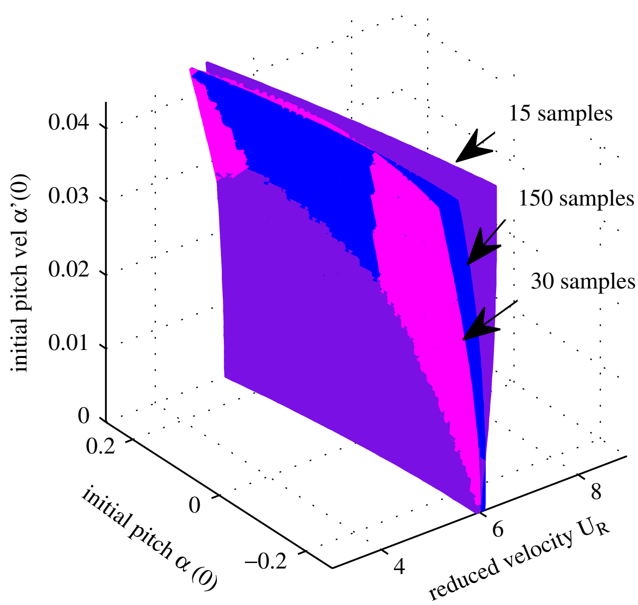

Fig. 14 Visualization of the convergence. The flutter boundary after 15, 30 and 150 samples have been evaluated through the high fidelity model

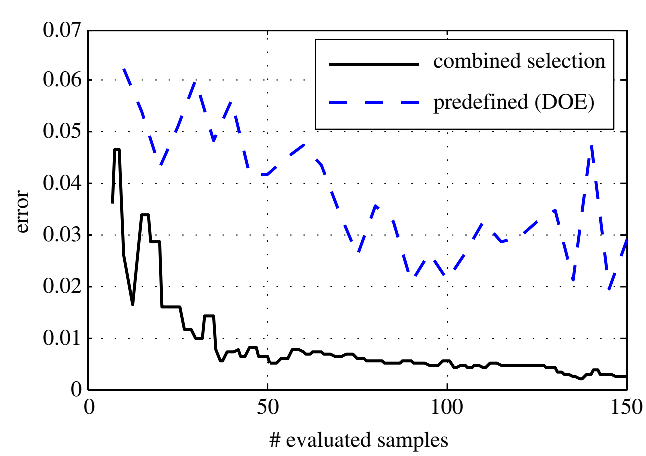

Fig. 16 Error of the three dimensional flutter boundary, with respect to the number of evaluated samples. The combination of approaches (*black curve*) leads consistently to a lower error than a simple DOE on the whole space (*dashed blue curve*)

asymptotically stable to the left of the boundary and limit-cycle oscillation occurs to the right of the boundary. As with the two-dimensional analytical problem, the three different methods of generating a new sample were used sequentially.

A total of 150 samples were evaluated. However, it appears that convergence was achieved at an earlier stage. Figure 13 shows the relative change of the high fidelity SVM for each new added sample. Figure 14 shows the flutter boundary at different states of the process. After evaluating 30 samples, the flutter boundary is, by visual inspection, close to the final result after 150 samples.

To obtain an approximation of the actual error a reference boundary was obtained as follows. A grid of 5,000 samples, with 10 samples along each initial condition and 50 samples along the reduced velocity parameter was evaluated through the high fidelity model. Based on these classified samples an SVM was created. Figure 15 shows this reference boundary and the approximated boundary obtained from the multifidelity scheme with 150 samples. The approximated boundary was compared to this reference boundary throughout the multifidelity process. Figure 16 shows this error measure with respect to the number of evaluated samples. The figure also depicts the error for a predefined design of experiments. For this problem, the multifidelity approach consistently leads to a smaller error.

5 Conclusion

This paper introduces a novel multifidelity approach for the construction of explicit boundaries with SVM. One of the key aspects of the methodology is the definition of a region (an envelope) encompassing a lower fidelity boundary in order to limit the number of high fidelity calls. In addition, pockets of inconsistency between the low and the high fidelity boundaries are identified and populated with a sample. The approach is combined with an already developed update scheme for the high fidelity model. The combination of approaches seems to provide the highest accuracy for a given number of samples.

The scheme is being applied to higher dimensional problems and a new approach for the refinement of the envelope is being investigated. In particular, the construction of the envelope based on information from the high fidelity SVM, in addition to the low fidelity one, is being studied.

Acknowledgments Part of this research was conducted in the context of a summer research program in the Air Vehicle Directorate of the Air Force Research Laboratory at Wright-Patterson Air Force Base through funding from Air Force Office of Scientific Research (Dr. Fariba Fahroo, Program Manager). The support of the National Science Foundation (award CMMI-0800117) is gratefully acknowledged for the research dealing with the Explicit Design Space Decomposition Methodology.

Appendix

A Stability analysis

In order to assess the stability of a given airfoil configuration, its response is studied in the time domain. This approach is essential in the case of "black-box" codes for which the Jacobian is not available. In addition, the study of the system's response is the only way to assess the true stability boundary (as opposed to based on a linear assumption) of a nonlinear system in the general case. In this study, the response considered is the mechanical energy defined as the sum of the kinetic and the elastic energies. This approach has the advantage of encompassing all the degrees of freedom of the system in one quantity. For an asymptotically stable system, the energy will converge. For an unstable

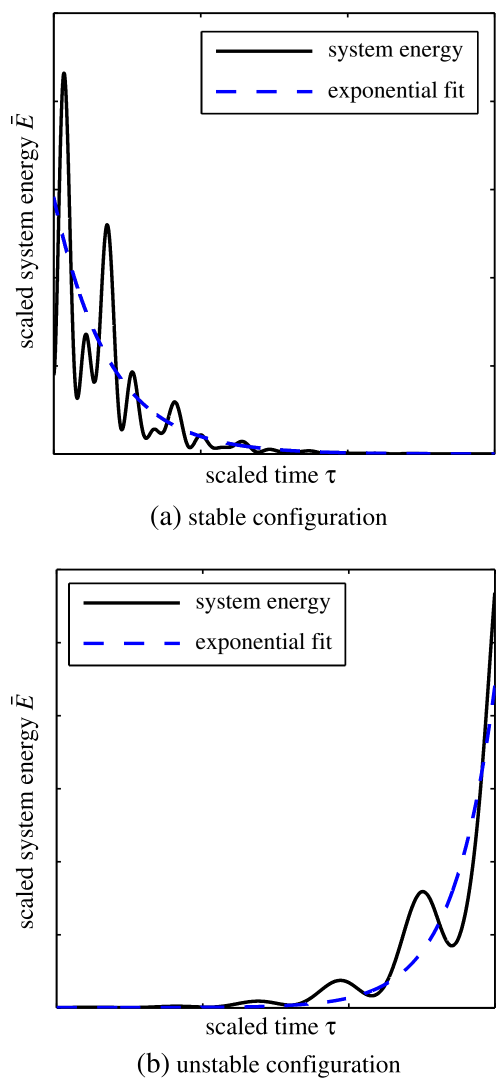

Fig. 17 Energy for a stable (**a**) and an unstable configuration (**b**). The *dashed line* represents an exponential least square approximation whose coefficient is either positive (unstable) or negative (stable)

system the system energy will continue to grow unboundedly. In order to capture the trend, the following function:

$$y(\tau) = p_1 e^{p_2 \tau} \tag{13}$$

with parameters p_1, p_2 approximates in a least square sense the mechanical energy. If p_2 is negative, the system is classified as stable, otherwise as unstable. Figure 17 provides examples of stable and unstable configurations. The system energy is calculated from the pitch and plunge velocities and the deformation of the springs. For the two DOF system the classification is not based on the system energy E directly, but on the dimensionless system energy $\bar{E}$ defined by:

$$\bar{E} = \frac{E}{\rho U^2 b^2} \tag{14}$$

Where U denotes the free stream velocity, ρ denotes the two-dimensional air density and b denotes the airfoil semi-chord. The restoring forces due to the springs are given in terms of plunge and pitch by:

$$F_h(\xi) = \xi + k_{3h}\xi^3 + k_{5h}\xi^5 \tag{15}$$

$$M_\alpha(\alpha) = \alpha + k_{3\alpha}\alpha^3 + k_{5\alpha}\alpha^5 \tag{16}$$

The energy stored in the spring in plunge is calculated as:

$$\bar{E}_{spring\,\xi} = \mu\pi \left(\frac{\omega}{U_R}\right)^2 \left(\frac{1}{2}\xi^2 + \frac{1}{4}k_{3h}\xi^4 + \frac{1}{6}k_{5h}\xi^6\right) \tag{17}$$

Similarly for the spring in pitch:

$$\bar{E}_{spring\,\alpha} = \mu\pi \left(\frac{r_\alpha}{U_R}\right)^2 \left(\frac{1}{2}\alpha^2 + \frac{1}{4}k_{3\alpha}\alpha^4 + \frac{1}{6}k_{5\alpha}\alpha^6\right) \tag{18}$$

The kinetic energies are calculated as:

$$\bar{E}_{kinetic\,\xi} = \frac{1}{2}\mu\pi\xi'^2 + 2x_\alpha\alpha'\xi'\cos(\alpha) + (x_\alpha\alpha')^2 \tag{19}$$

$$\bar{E}_{kinetic\,\alpha} = \frac{1}{2}\mu\pi U_R^2\alpha'^2 \tag{20}$$

Where the prime sign for the degrees of freedom represents the derivative with respect to the non-dimensional time.

References

Alexandrov NM, Nielsen EJ, Lewis RM, Anderson WK (2000a) First-order model management with variable-fidelity physics applied to multi-element airfoil optimization. Tech. rep., Nasa Langley Research Center

Alexandrov NM, Lewis RM, Gumbert CR, Green LL, Newman PA (2000b) Optimization with variable-fidelity models applied to wing design. Tech. rep., Nasa Langley Research Center

Alpaydin E (2004) Introduction to machine learning. MIT Press, Cambridge

Balabanov V, Haftka RT, Grossman B, Mason WH, Watson LT (1998) Multifidelity response surface model for HSCT wing bending material weight. In: 7th AIAA/USAF/NASA/ISSMO symposium on multidisciplinary analysis and optimization, AIAA-1998-4804, pp 778–788

Basudhar A, Missoum S (2008) Adaptive explicit decision functions for probabilistic design and optimization using support vector machines. Comput Struct 86(19–20):1904–1917. doi:10.1016/j.compstruc.2008.02.008

Basudhar A, Missoum S (2009) A sampling-based approach for probabilistic design with random fields. Comput Methods Appl Mech Eng 198(47–48):3647–3655

Basudhar A, Missoum S, Sanchez AH (2008) Limit state function identification using support vector machines for discontinuous responses and disjoint failure domains. Probab Eng Mech 23(1):1–11. doi:10.1016/j.probengmech.2007.08.004

Cristianini N, Schölkopf B (2002) Support vector machines and kernel methods: the new generation of learning machines. Artif Intell Magazine 23(3):31–41

Eldred MS, Dunlavy DM (2006) Formulations for surrogate-based optimization with data-fit, multifidelity and reduced-order models. In: 11th AIAA/ISSMO multidisciplinary analysis and optimization conference, AIAA-2006-7117

Eldred MS, Giunta AA, Collis SS, Alexandrov NA, Lewis RM (2004) Second-order corrections for surrogate-based optimization with model hierarchies. In: Proceedings of the 10th AIAA/ISSMO multidisciplinary analysis and optimization conference, AIAA-2004-4457

Gano S, Renaud J, Sanders B (2005) Hybrid variable fidelity optimization by using a kriging-based scaling function. AIAA J 43(11):2422–2433. doi:10.2514/1.12466

Gano S, Renaud J, Martin J, Simpson T (2006) Update strategies for kriging models used in variable fidelity optimization. Struct Multidisc Optim 32(4):287–298. doi:10.1007/s00158-006-0025-y

Harrison A, Missoum S, Martinez J (2006) Design space decomposition using support vector machines for reliability-based design optimization. In: 11th symposium AIAA/ISSMO on multidisciplinary analysis and optimization, AIAA-2006-6927

Keane A (2003) Wing optimization using design of experiment, response surface, and data fusion methods. J Aircr 40(4):741–750

Layman R, Missoum S, Geest J (2007) Failure prediction and robust design of grafts for aortic aneurysms. In: 48th AIAA/ASME/ASCE/AHS/ASC structures, structural dynamics, and materials conference, AIAA-2007-1888

Lee BHK, Jiang LY, Wong YS (1999) Flutter of an airfoil with cubic restoring force. J Fluids Struct 13(1):75–101

Lucia DJ, Beran PS, Silva WA (2004) Reduced-order modeling: new approaches for computational physics. Prog Aerosp Sci 40(1–2):51–117. doi:10.1016/j.paerosci.2003.12.001

Madsen J, Langthjem M (2001) Multifidelity response surface approximations for the optimum design of diffuser flows. Optim Eng 2(4):453–468. doi:10.1023/A:1016046606831

Mason B (1998) Variable complexity design of composite fuselage frames by response surface techniques. Thin-Walled Struct 32(4):235–261. doi:10.1016/S0263-8231(98)00016-0

Missoum S, Ramu P, Haftka RT (2007) A convex hull approach for the reliability-based design optimization of nonlinear transient dynamic problems. Comput Methods Appl Mech Eng 196(29–30):2895–2906. doi:10.1016/j.cma.2006.12.008

Missoum S, Beran P, Kurdi M, McFarland M (2008) Reliability-based design optimization of nonlinear aeroelastic problems. In: 49th AIAA/ASME/ASCE/AHS/ASC structures, structural dynamics, and materials conference, AIAA-2008-2075

Robinson T, Willcox K, Eldred M, Haimes R (2006) Multifidelity optimization for variable-complexity design. In: 11th AIAA/ISSMO multidisciplinary analysis and optimization conference, AIAA, AIAA, AIAA-2006-7114

Romero V, Burkardt J, Gunzburger M, Peterson J (2006) Comparison of pure and latinized centroidal voronoi tesselation against various other statistical sampling methods. J Reliab Eng Syst Saf 91:1266–1280

Seydel R (1988) From equilibrium to chaos: practical bifurcation and stability analysis. Elsevier Science, Amsterdam

Simpson TW, Toropov V, Balabanov V, Viana FAC (2008) Design and analysis of computer experiments in multidisciplinary design optimization: a review of how far we have come–or not. In: 12th AIAA/ISSMO multidisciplinary analysis and optimization conference, AIAA-2008-5802

Toropov VV, Markine VL (1996) The use of simplified numerical models as mid-range approximations. In: 6th AIAA/USAF/NASA/ISSMO symposium on multidisciplinary analysis and optimization, AIAA-1996-4088

Venkataraman S, Haftka RT, Johnson TF (1998) Design of shell structures for buckling using correction response surface approximations. In: 7th AIAA/USAF/NASA/ISSMO symposium on multidisciplinary analysis and optimization, AIAA-1998-4855

Vitali R, Haftka RT, Sankar BV (1998) Correction response surface approximations for stress intensity factors of a composite stiffened plate. In: 39th AIAA/ASME/ASCE/AHS/ASC structures, structural dynamics and materials conference, AIAA-1998-2047, pp 2917–2922